coatings

MDPI

Article

Pulsed Laser Deposition of Epitaxial Non-Doped $PbTiO_3$ Thin Films from PbO–TiO_2 Mosaic Targets

Joe Sakai *, José Manuel Caicedo Roque, Pablo Vales-Castro, Jessica Padilla-Pantoja, Guillaume Sauthier and José Santiso

Institut Català de Nanociència i Nanotecnologia (ICN2), CSIC and The Barcelona Institute of Nanoscience and Nanotechnology (BIST), UAB Campus, 08193 Bellaterra, Spain; jose.caicedo@icn2.cat (J.M.C.R.); pablo.vales@icn2.cat (P.V.-C.); jessica.padilla@icn2.cat (J.P.-P.); guillaume.sauthier@icn2.cat (G.S.); jose.santiso@icn2.cat (J.S.)

* Correspondence: sakai.joe@gmail.com

Abstract: $PbTiO_3$ (PTO) suffers from difficulty in preparing high-density robust bulk ceramics, which in turn has been a bottleneck in thin films growth with physical vapor deposition (PVD) methods. In the present work, we prepared non-doped PTO thin films by a pulsed laser deposition (PLD) method with either a single PTO target or a mosaic target consisting of PbO and TiO_2 pie-shaped pieces. On the PTO single target, laser irradiation caused selective ablation of Pb, resulting in Ti-rich cone-shaped pillar structure on the surface, whereas the irradiated surface of PbO and TiO_2 pieces was smoother. Epitaxial PTO films deposited on $SrTiO_3$ (001) substrates from the pie-chart targets with PbO:TiO_2 areal ratio from 3:5 to 5:3 resulted in composition, crystallinity, flatness, and ferroelectric properties almost independent of the areal ratio. The averaged composition of each film was close to stoichiometric, suggesting a compositional self-control mechanism. For growing epitaxial and high-quality non-doped PTO films, a PbO–TiO_2 pie-chart target is advantageous in easiness of handling and stable surface structure.

Keywords: pulsed laser deposition; ferroelectric material; lead titanate; mosaic target; sequential ablation; compositional self-control mechanism

Citation: Sakai, J.; Roque, J.M.C.; Vales-Castro, P.; Padilla-Pantoja, J.; Sauthier, G.; Santiso, J. Pulsed Laser Deposition of Epitaxial Non-Doped $PbTiO_3$ Thin Films from PbO–TiO_2 Mosaic Targets. *Coatings* **2021**, *11*, 662. https://doi.org/10.3390/coatings11060662

Academic Editor: Oleksandr Tkach

Received: 9 May 2021
Accepted: 29 May 2021
Published: 31 May 2021

1. Introduction

$PbTiO_3$ (PTO) is a pioneering and still important ferroelectric material with a perovskite-type structure [1,2]. The crystalline structure of PTO is cubic at temperatures above 490 °C, whereas it is tetragonal at lower temperatures with a large *c*/*a* ratio of 1.06 at room temperature (RT) [1]. The significant structural phase transition often causes cracks in the whole volume of PTO bulk ceramics during cooling after sintering at a higher temperature. This makes the PTO bulk ceramics extremely fragile, which in turn is a difficulty for using it as a target material typically needed in thin films growth processes by physical vapor deposition (PVD) techniques. To overcome this fragility, one popular solution is using sintering aids or doping with other elements to form "modified PTO" [3,4].

Another factor that could make the growth of PTO thin films difficult is the high vapor pressure of lead oxide. In general, PLD method allows thin films growth with cation composition close to that of the target. However, when the material contains a volatile element, it is often observed that film composition progressively deviates from stoichiometry because of the volatile element depletion when depositing at elevated temperatures [5]. Many groups growing PTO films by PVD techniques with a single PTO target attempt to prevent the Pb deficiency with strategies that can be categorized into two, namely, to mitigate the re-evaporation of Pb from the growing film or to supply species with an excess Pb/Ti ratio onto the substrate to compensate for the Pb loss. The practical deposition conditions based on the former strategy include (a) low substrate temperature (550 °C or lower) [6–8], and (b) high oxygen ambient pressure (100 mTorr or higher) [7,9–14]. A

common strategy for the latter category is (c) to use a Pb-rich target [6,7,10,15], although the exact amount of Pb in excess will depend on the deposition conditions.

Supplying species from two targets has been reported to effectively function for preparing high-quality thin films containing a high vapor-pressure element. The alternative ablation of two (or more) targets has been regularly employed since the beginning of combinatorial PLD researches [16,17]. The species sequentially ablated from multiple targets are expected to mix on the growing surface to form a uniform film provided that the individual layer thickness for each cycle is at the monolayer level to allow for intermixing. In that way, the ratio of species supplied from multiple targets can be controlled by modifying the number of laser pulses on each target. However, this method typically results in a larger setup complexity due to the need for constant exchange of target positions (or laser redirecting to the different targets) and result in an overall reduced growth rate. This can be regarded as an advanced technique belonging to category (c). In this way, Maruyama et al. have succeeded in obtaining epitaxial $LiCoO_2$ thin films by alternative laser ablation of Li_2CO_3 and CoO targets [18]. A similar approach by using the simultaneous ablation of two targets (with two independent lasers or a split laser beam) can also be a powerful tool for this purpose, in this case avoiding continuous target exchange [19,20]. In this manner, Hussey and Gupta have prepared good quality $YBa_2Cu_3O_{7-d}$ (YBCO) films by simultaneously shedding laser beams to individual YBa_2O_x and CuO targets [21].

A much simpler approach for sequential ablation is based on using a mosaic target consisting of pieces of multiple materials, which requires only one rotating target [5]. Since PLD film growth rates produce sub-monolayer thickness per pulse (typically below 1 Å/pulse depending on the deposition conditions, namely laser fluence, gas pressure and target-to-substrate distance), the number of pulses in each part of the target at standard target rotation speeds produce a sequence of very short pulses allowing for homogenous cross plane composition. Besides, the possible composition inhomogeneities caused by slight variations in the sequence, or when ablating at the boundary regions between both compounds in the target, are averaged during film growth and expected to produce negligible effects. In this way, Lee et al. have demonstrated to compensate the typical Zn deficiency in the PLD growth of $ZnGa_2O_4$ (ZGO) films at high temperature by using a mosaic target consisting of ZGO and ZnO [22]. The mosaic target strategy has been successfully adopted to deposit PTO films, since both PbO and TiO_2 are robust ceramics unlike PTO. Funakoshi et al. have already performed PLD of PTO polycrystalline films on silicon (Si) substrates using a PbO–TiO_2 mosaic target [23]. Nothing precludes the use of this method for growing PTO epitaxial films, except for the larger difficulty due to the need of higher deposition temperatures to achieve crystalline order. However, to our knowledge, there has been no previous report on the growth of epitaxial PTO films using a mosaic target.

In the present study, we prepared epitaxial PTO films on perovskite-type oxide single-crystal substrates with PLD. Either a mosaic target consisting of PbO and TiO_2 pie-shaped pieces or, for comparison, a single PTO target was employed. A cone-shaped pillar structure, accompanied by Pb-deficient composition, was observed on the surface of the single PTO target after laser irradiation and supposed to impede the reproducible Pb/Ti ablation during deposition. PTO epitaxial films were grown from a series of pie-chart targets resulting in composition, crystallinity, flatness, and ferroelectric properties comparable with the film obtained from a single PTO target.

2. Experiments

2.1. Fabrication and Characterization of Targets

To prepare the $PbTiO_3$ target, mixed powders of PbO and TiO_2 were pressed in 30 mm-diameter dies, and calcinated in air at 800 °C for 1 h. No sintering aids were used in this case. The product was ground and re-pressed and sintered in air at 1160 °C for 2 h. The bulk was extremely fragile so that it easily breaks when picked up with tweezers. On the other hand, individual PbO and TiO_2 targets were prepared by pressing the powder

in the 30 mm-diameter dies and sintering in air at 750 °C for 1 h, and at 1200 °C for 6 h, respectively. Both PbO and TiO_2 disks thus obtained were robust. The 3 mm-thick disks were then cut into quarter circle or one-eight circle shape with a diamond saw. The pie-shaped pieces were fixed on an aluminum disk with a double-sided carbon tape in various PbO:TiO_2 areal ratios of 3:5, 4:4, and 5:3 (Figure 1a).

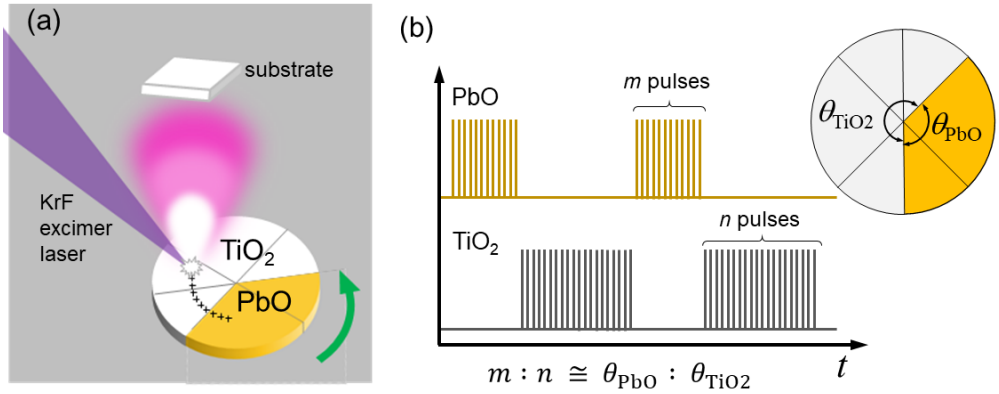

Figure 1. Schematics of PLD using a PbO–TiO_2 pie-chart target. (**a**) Configuration of pie-chart target, laser spot, and substrate. The laser spot is off-centered with respect to rotation axis of the target. (**b**) Sequence of PbO and TiO_2 ablation.

A commercial (Nb,Mg)-modified $Pb_{1.1}TiO_3$, much denser, was also used from comparison (Nb and Mg are sintering aids). The laser-induced evolution of surface morphology and composition was studied for the homemade $PbTiO_3$ target, as well as for the commercial $Pb_{1.1}TiO_3$, and the homemade PbO/TiO_2 targets. For this, the target surface was irradiated by a focused excimer laser (COMPex 102, KrF gas, wavelength of 248 nm, Lambda Physik, Göttingen, Germany) beam at different fluence in 100 mTorr oxygen pressure. The morphology and the composition of the target surface was observed with a scanning electron microscopy (SEM, Quanta 650 FEG, FEI, Hillsboro, OR, USA) and an energy-dispersive X-ray (EDX) spectroscopy (X-Max, Oxford Instruments, High Wycombe, UK), respectively.

2.2. Thin Films Growth

PTO thin films were grown mainly on single-crystal $SrTiO_3$ (STO; 001) substrates using either the PTO single target or the PbO–TiO_2 pie-chart target. The STO substrates were chemically and thermally pre-treated to form atomically flat surface with a step (~4 Å height) and terrace structure [24]. The deposition conditions for PTO films were as follos: substrate temperature of 550 °C, ambient oxygen pressure of 100 mTorr, laser repetition rate of 2 Hz, total pulse number of 1760, energy on the target surface of 50 mJ, fluence of 1.3 J/cm^2, and target–substrate distance of 50 mm. As a bottom electrode layer for electrical characterization, a 15 nm-thick $La_{0.6}Sr_{0.4}MnO_3$ (LSMO) layer was deposited with deposition conditions of 650 °C, 100 mTorr, 2 Hz, 740 pulses, 50 mJ, 2.0 J/cm^2, and 50 mm, prior to the PTO layer growth. The target rotates with a speed of 3 rpm during laser irradiation. Rastering, as well as rotation, were used on the single PTO and LSMO targets for uniform ablation [25], whereas only rotation (no rastering) was used on the mosaic targets. After the deposition, the sample was cooled to room temperature at a rate of −10 °C/min in O_2 ambient of 10 Torr. Hereafter, we label the PTO/LSMO/STO samples prepared with the pie-chart target with the PbO:TiO_2 areal ratios of 3:5, 4:4, and 5:3 as samples PC35, PC44, and PC53, respectively, and the one with the single PTO target as sample SP. The actual pulse numbers fed to PbO and TiO_2 pieces during one cycle of rotation are shown in Table 1. The deviation of pulse numbers ratio from the central angle ratio between PbO and TiO_2, which should theoretically be identical (Figure 1b), is due to a slight offset between the target center and the rotation axis.

Table 1. Deposition parameters and characteristics of four samples.

Sample Name	$PbO:TiO_2$ Areal Ratio	Number of Pulses Irradiated on $PbO:TiO_2$ per 1 Cycle	PTO Growth Rate (10^{-3} nm/pulse)	PTO out-of-Plane Lattice Spacing (Å)	PTO 002 Rocking Curve FWHM (deg)
SP	-	-	28	4.158	0.080
PC35	3:5	12:30	15	4.146	0.081
PC44	4:4	18:24	14	4.146	0.087
PC53	5:3	24:18	8.6	4.141	0.090

2.3. Characterization of Films

Crystallinity of PTO films was evaluated with 2θ–ω scans, rocking curves and reciprocal space mapping (RSM) by X-ray diffraction (XRD) using a diffractometer with a four-circle goniometer (X'pert PRO-MRD, Malvern-PANalytical, Almelo, The Netherlands). Surface morphology was observed with atomic force microscopy (AFM). X-ray photoemission spectroscopy (XPS) and Rutherford backscattering spectroscopy (RBS) were employed to characterize the composition of the PTO films. XPS measurements were performed at RT with a hemispherical analyzer (PHOIBOS 150, SPECS, Berlin, Germany). Here, calculation of the Pb ratio, defined as Pb/(Pb + Ti), was based on three different Pb lines, namely 4d (binding energies 413 and 435 eV), 4f (138 and 143 eV), and 5d (20 and 22 eV), and one Ti line 2p (455 and 461 eV). Due to the different binding energies, the three Pb lines give the signals originating from surface layers of different thicknesses. This was used to account for possible Pb composition gradients at the surface. The RBS measurement was performed with a tandem accelerator at Centro de Micro-Análisis de Materiales, Madrid, Spain. He^+ ions of an energy of 2 MeV were directed to the sample at an angle of 2.8° from the normal direction, and the scattered particles were detected at an angle of 165° with respect to the incident angle. The ferroelectric properties of the films were evaluated through phase–bias curves and write–erase tests using a piezoresponse force microscopy (PFM) system. Both AFM and PFM were carried out using a scanning probe microscopy system (MFP-3D Classic, Asylum Research, Santa Barbara, CA, USA). See [20] for the detail of XRD, XPS, and PFM procedures.

3. Results

3.1. Morphology and Composition of the Target Surface

Surface SEM images of a commercial (Nb,Mg)-doped $Pb_{1.1}TiO_3$ target are shown in Figure 2a–c. The non-irradiated pristine region (Figure 2a) consists of random-shaped grains of several tens' micrometers. Adjacent grains are weakly connected, resulting in an overall porous structure. Cone-shaped pillars appeared on the surface of the target immediately after irradiation of a few laser shots. The pillars pointed to the direction of laser incidence (Figure 2b). The surface after being used for several tens of depositions with fluence of 1 to 2 J/cm^2 shows significant cone-shaped pillars at the level of several tens of micrometers (Figure 2c). EDX analysis revealed Ti-rich (Pb-poor) composition on the surface with such a pillar structure. The off-stoichiometry suggests that selective ablation of Pb has occurred due to its high vapor pressure, leaving Ti component on the surface. This cone-shaped pillar structure looks similar to the one generated on a YBCO target [26]. The pillars on the YBCO bulk were reported to be Cu-poor and Y-rich, and was generated when the laser fluence was below a threshold of 1 J/cm^2 [26]. In the case of PTO, unlike YBCO, the off-stoichiometry remained in any fluence examined in the experiment, from 0.3 to 4.7 J/cm^2.

Figure 2d,e shows SEM images of the homemade PTO target. The pristine surface, even though flatter than the commercial $Pb_{1.1}TiO_3$ target, is filled with microcracks that explain its fragility (Figure 2d). Appearance of cone-shaped pillars due to laser irradiation (Figure 2e) was not as remarkable as that on the commercial target shown in Figure 2b. Still, this target was not free from a compositional shift towards Pb-poor values. Figure 2f shows the relationship between the laser fluence and the Pb ratio in the commercial (Nb,Mg)-

doped $Pb_{1.1}TiO_3$ and the homemade $PbTiO_3$ targets. In both cases, large deviations from the initial composition were observed down to about Pb/(Pb + Ti) = 0.4. Although deviation tends to reduce as the fluence increases after a minimum point, it is not completely suppressed. Similar surface morphology observations were carried out for the bulk targets of the binary oxides PbO and TiO_2. The PbO surface was quite flat and crack-free either at pristine state (Figure 3a) or after laser irradiation (Figure 3b). TiO_2, initially consisting of ~10 μm-sized grains (Figure 3c), was deformed by the laser to show a 3d structure, wavy rather than pillarlike (Figure 3d).

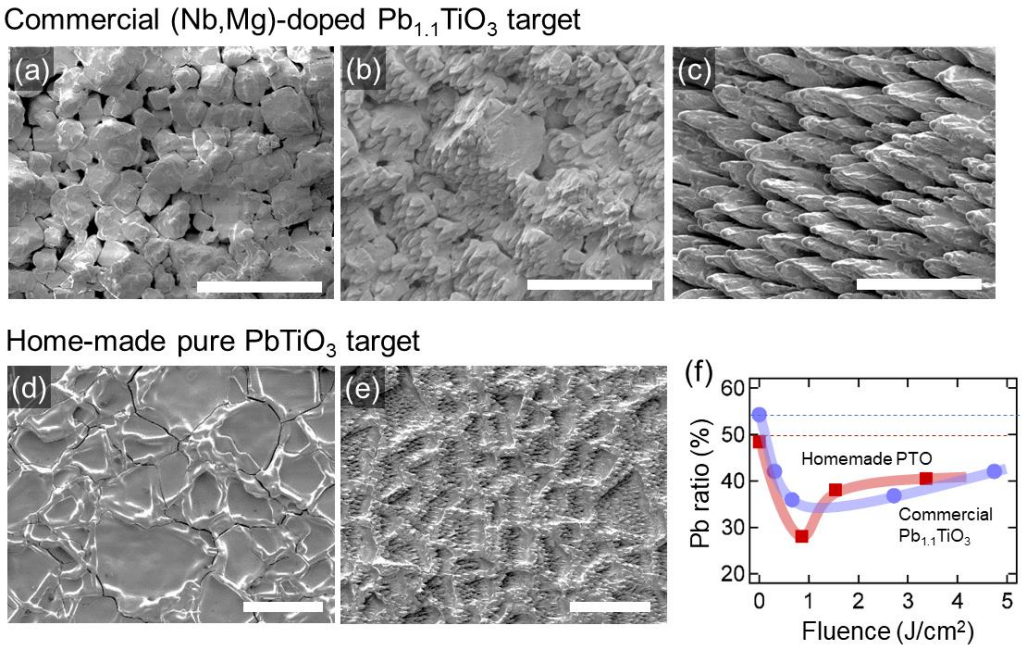

Figure 2. SEM images of (**a**–**c**) a commercial (Nb,Mg)-doped $Pb_{1.1}TiO_3$ target and (**d**,**e**) a homemade pure $PbTiO_3$ target. (**a**) Pristine. (**b**) Irradiated with 50 pulses of laser with a fluence of 0.3 J/cm^2 while the target was fixed. (**c**) After used for several tens of depositions with fluence of 1 to 2 J/cm^2. (**d**) Pristine. (**e**) Irradiated with 50 pulses of laser with a fluence of 0.9 J/cm^2 while the target was fixed. Scale bars correspond to 50 μm in (**a**–**c**) and 100 μm in (**d**,**e**). (**f**) Pb ratio of commercial $Pb_{1.1}TiO_3$ and homemade $PbTiO_3$ target surface after 50 pulses of irradiation as a function of laser fluence. Dashed lines represent the designed composition of each target.

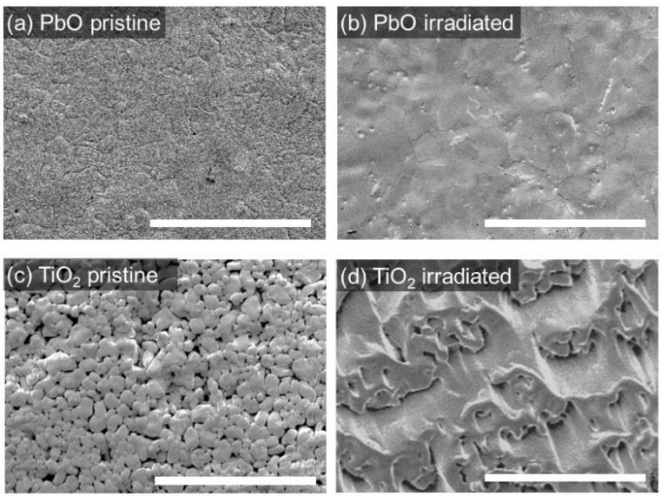

Figure 3. SEM images of (**a**,**b**) PbO and (**c**,**d**) TiO_2 target surfaces, (**a**,**c**) pristine and (**b**,**d**) after used for several depositions with fluence of 1 to 2 J/cm^2. Scale bars correspond to 100 μm for all panels.

3.2. Properties of PTO Films

XRD 2θ–ω scans around STO 002 reflection of samples SP, PC35, PC44, and PC53 are shown in Figure 4a. In all the samples, the PTO 002 diffraction peak was accompanied by Laue fringes, which indicate high crystallinity of the PTO layer. Thickness of the PTO layer was estimated from the fringe interval to be 32.7, 26.8, 24.1, and 15.2 nm for samples SP, PC35, PC44, and PC53, respectively. The growth rate of the PTO layer (Table 1) was highest in sample SP and lowest in sample PC53. The slight difference in the cell parameters (Table 1) can qualitatively be explained through the difference of degree of strain originating in the thickness variation. The rocking curves around the PTO 002 reflection in the four samples showed FWHM smaller than 0.1°, the ones of SP and PC35 being slightly smaller than the others (Figure 4b, Table 1). The epitaxial relationship between films and substrate was confirmed with RSM, as shown in Figure 4c. The spots corresponding with PTO, LSMO, and STO are aligned vertically, indicating the in-plane lattice of the films fully coherent to the substrate.

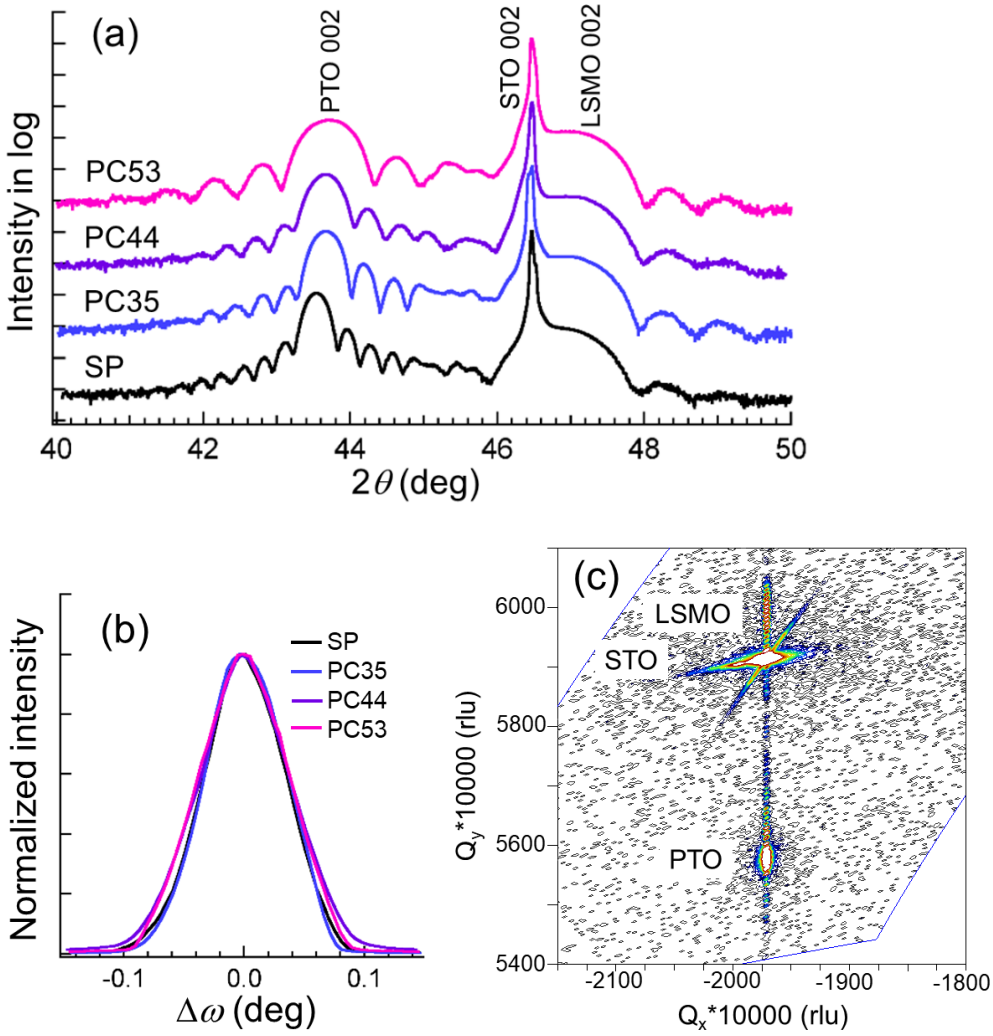

Figure 4. (**a**) XRD 2θ–ω profiles around STO 002 diffraction of samples SP, PC35, PC44, and PC53. The profiles are offset for clarity. (**b**) XRD rocking curves around PTO 002 diffraction of the four samples. (**c**) RSM of sample PC35 around (−103) diffraction of STO, PTO, and LSMO.

AFM topographic images of the four samples are shown in Figure 5. All the images show lines corresponding to the terraces on the STO substrates. The peak-to-valley values were within 1 nm in the 5×5 μm^2 area for all the samples.

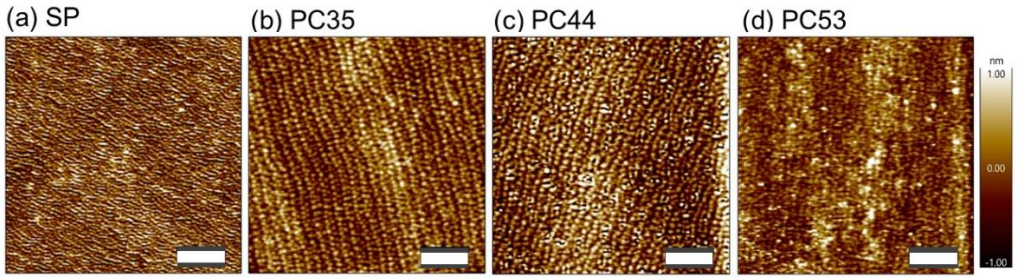

Figure 5. AFM topographic images of samples (**a**) SP, (**b**) PC35, (**c**) PC44, and (**d**) PC53. Scale bars correspond to 1 μm. Color scale (right-hand side of **d**) is common for all four images.

The results of XPS analysis of four samples are reported in Figure 6. Unexpectedly, the Pb ratio in the PTO layers was found to be quasi-consistent among the four samples. Meanwhile, the calculated Pb composition strongly depended on the Pb lines used for the evaluation. The Pb lines with higher binding energy resulted in the Pb ratio closer to stoichiometry. Generally, the higher the binding energy, the thicker the surface layer probed. Therefore, the dependence of Pb ratio suggests the possibility of Pb segregation in PTO layers towards the surface. The Pb ratio larger than 50% even for the highest binding energy line (Pb 4d) implies that the thickness of Pb segregation was larger than the XPS observation depth (a few nanometers). The composition difference among the samples was negligible compared with the evolution along the depth.

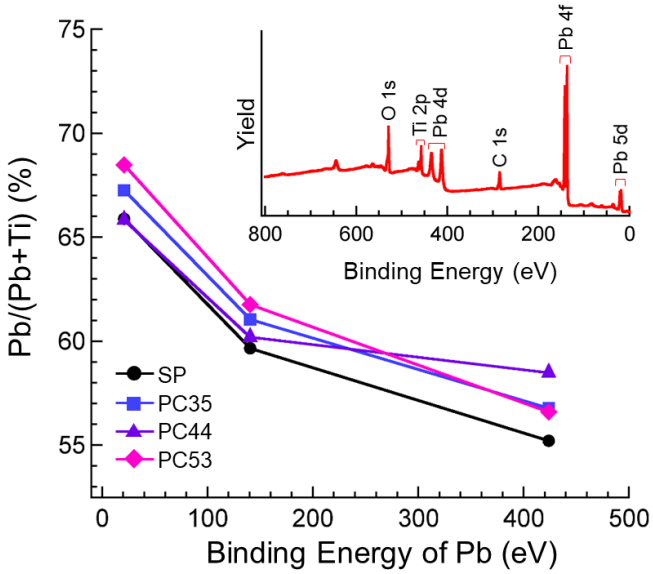

Figure 6. Pb ratio of four samples deduced using XPS signals of various Pb lines as functions of binding energy of the Pb lines. Inset shows a wide-range XPS profile of sample PC35.

We also carried out RBS characterization for two PTO films grown for this purpose, one directly on a STO substrate using the single PTO target and the other on a CeO_2-buffered r-plane sapphire (Al_2O_3 ($1\bar{1}02$)) substrate using the pie-chart target of PbO:TiO_2 = 4:4. The Al_2O_3 substrate was chosen so that the Ti signals from the film would be completely separated from signals from the substrate. The film on CeO_2/Al_2O_3 ($1\bar{1}02$) was regarded to be quasi-epitaxial since the PTO layer was confirmed to be (*h*00) oriented. The RBS analysis suggested Pb ratio of 49% and 50% for the whole thickness of the PTO layers in PTO/STO and PTO/CeO_2/Al_2O_3 samples, respectively (Figure 7). As the composition analyzed with XPS was consistent among the four samples grown on LSMO/STO, we speculate that the averaged Pb ratio of ~50% is adopted for all the samples.

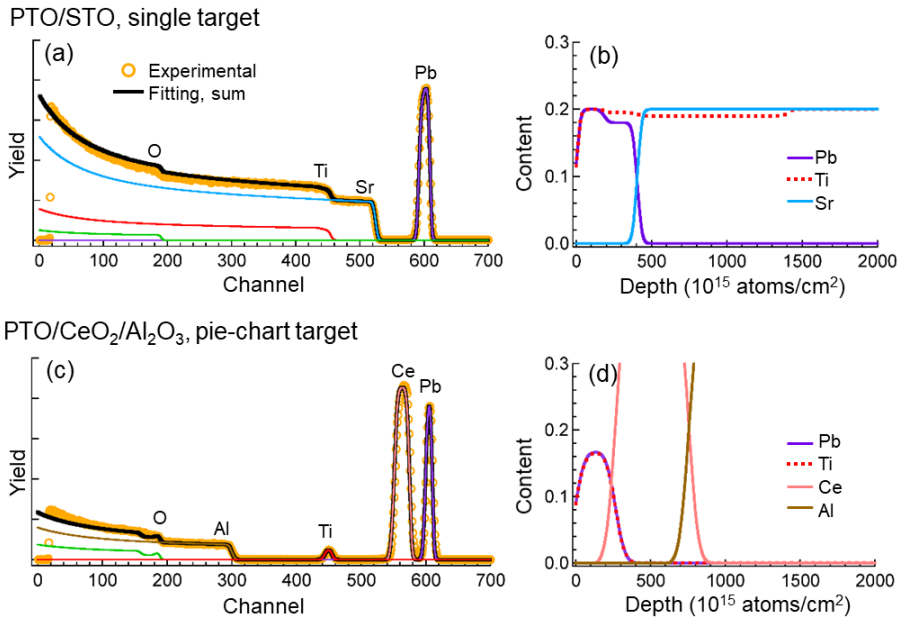

Figure 7. RBS profiles of PTO films deposited on (**a**) a STO substrate using a single PTO target, and (**c**) a CeO_2-buffered r-Al_2O_3 substrate using a 4:4 pie-chart target. Experimental data and simulated curves are overlapped. Depth profiles deduced from the RBS simulation results of (**b**) PTO/STO and (**d**) PTO/CeO_2/Al_2O_3 samples. The depth profiles of Pb and Ti are completely overlapped in (**d**).

In order to confirm the ferroelectric properties of the four samples, write–erase test in a few micrometers' square region and phase–bias measurement was performed using PFM. As shown in Figure 8, all samples showed good write and erase characteristics and typical phase–bias curves, which prove good ferroelectricity for all the PTO films.

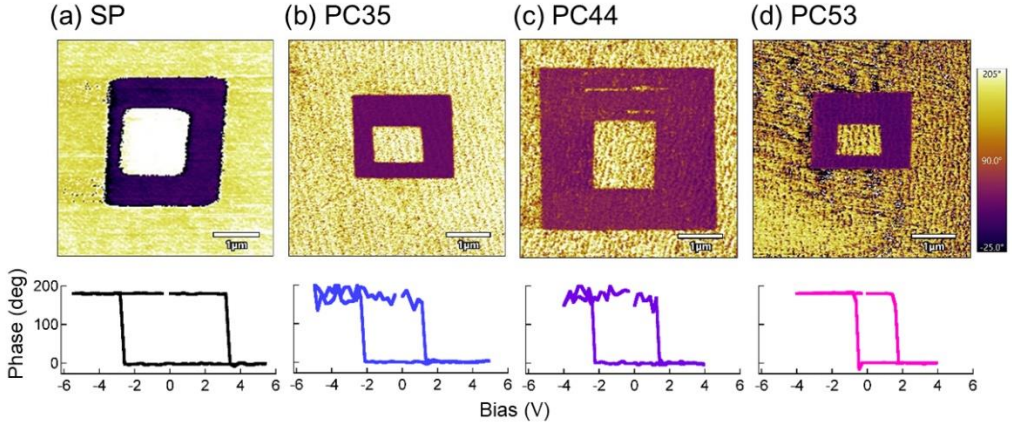

Figure 8. PFM write–erase images (top) and phase–bias curves (bottom) of samples (**a**) SP, (**b**) PC35, (**c**) PC44, and (**d**) PC53. Color scale (right-hand side of **d**) is common for the four PFM images.

4. Discussion

In a binary oxide (AO_x) target the only possible composition deviation among the ablated species is the ratio x of O to A, which can be compensated through the oxygen ambient pressure. Furthermore, deposition using PbO and TiO_2 bulks, free from cone-shaped pillars, is desirable in terms of reproducibility in film growth. The appearance of cone-shaped pillars could perturb the distribution of local laser fluence, which could drastically affect not only the ablation rate, and therefore the film growth rate, but also the quality of the film.

The composition of the PTO layers, independent of the areal ratio of the pie-type PbO and TiO_2 pieces, indicates that a compositional self-control (CSC) mechanism occurs

during film growth. The CSC mechanism has been reported in PZT thin films grown on $Pt/Ti/SiO_2/Si$ substrates with a sputtering method [27]. Provided that the deposition rate is not too high, as in the present case, the adatoms are allowed to migrate over the substrate or growing film surface. They will be crystallized to form a stoichiometric crystal with Pb:(Ti + Zr) equal to 1:1 or, if they are in excess, will be re-evaporated. The present result confirmed that this should have occurred for the A cations excess (Pb). Not incorporated into the perovskite structure, the excess Pb segregated towards the surface and ultimately was re-evaporated. Most probably, composition of the adatoms fed to the substrate was the closest to stoichiometric in PC35, resulting in the highest growth rate and the smallest FWHM, whereas it was the farthest in PC53 with the lowest growth rate. The growth rate variation among samples is quite consistent with the TiO_2 supply rate (ratio in growth rate between PC35 and PC53 was 1.7, exactly the same as the ratio in number of TiO_2 pulses/target turn between them; see Table 1). This suggests that Pb was always in excess, and is expelled from the film in the CSC mechanism. Similarly, It was also the CSC mechanism that resulted into stoichiometric films when deposited from the single PTO target on which Pb is selectively ablated (see Section 3.1).

It would be informative to compare the present results with those by Funakoshi et al. [23]. In their PTO films grown on Si substrates, Pb/Ti was 2.59 (i.e., Pb ratio 72%) when PbO and TiO_2 pieces were irradiated with the same number of laser pulses, whereas the pulse numbers ratio of 29:71 to $PbO:TiO_2$ resulted in a stoichiometric PTO film. The Ti deficiency in the former film could be due to the difference of the deposition rate between PbO and TiO_2 pieces. In the present study on epitaxial films, stoichiometric films were obtained when the pulse number ratio of $PbO:TiO_2$ was at least in the range of 12:30 (=29:71) to 24:18 (=57:43). The difference clearly originated in the difference between perovskite-type single crystal substrates that promote epitaxial growth and Si substrates that do not. The best film in terms of crystallinity (PC35) was obtained with a pulse numbers ratio of 29:71, which was in agreement with the result of Funakoshi et al. It should be noted that PTO films deposited on Si substrates in the present study, from either PTO or pie-chart target during the same runs as those on STO, have always resulted in Pb-rich composition in EDX analysis (not shown). We attribute this difference to whether the CSC mechanism functioned or not depending on STO or Si substrates, rather than to the difference of the analysis techniques.

The composition of a PTO film prepared by PLD would be affected by the balance among multiple factors such as:

(i) selective ablation at the target (which would drive the film composition to Pb-rich);
(ii) re-evaporation from the substrate (to Pb-poor);
(iii) the CSC mechanism (to stoichiometry).

In the case of epitaxial films grown in O_2 of 100 mTorr at 550 °C, the effect of (iii) was revealed to be more significant than (i) and (ii), meaning that the laser-induced off-stoichiometry on the single PTO target is not a severe issue in the composition viewpoint. However, the pie-chart target, which can compensate for the composition deviation due to the effect of (i), is useful when one attempts to deposit PTO films in a non-epitaxial manner. The robustness and pillar-free surface are also the advantages of the pie-chart target over the PTO target. The pie-chart target strategy would be generally applicable to materials containing elements with high vapor pressure, and probably to other physical vapor deposition techniques such as sputtering.

5. Conclusions

Irradiation of a PTO target with a pulsed laser beam of any fluence causes selective ablation of Pb, which induces a Ti-rich cone-shaped pillar structure, affecting the stability and composition control of the thin film deposition process. On the other hand, the PbO and TiO_2 targets are robust and free from cone-shaped pillars after laser irradiation. This allows for a better control of the deposition process.

We prepared PTO thin films by the PLD method using either a PbO–TiO_2 pie-chart targets or PTO single target. On STO (001) substrates, which allow the epitaxial growth, the PbO–TiO_2 pie-chart target with the areal ratio from 3:5 to 5:3 provided films with composition, crystallinity, flatness, and ferroelectric properties almost independent of the areal ratio. Even the PTO single target produced films with properties similar to those from pie-chart targets, despite the surface off-stoichiometry caused by the laser irradiation history. To explain this coincidence a compositional self-control (CSC) mechanism was suggested to occur during the growth of epitaxial PTO films.

In conclusion, the use of PbO–TiO_2 pie-chart target produces high-quality epitaxial films comparable to the ones from a PTO single target. The advantages of the pie-chart target include the robustness of the target and the long-term controllability of ablated compositions. In the preparation of films containing volatile species (Pb, Bi, Zn, Sn, Li, . . .) by PVD methods, the mosaic-target scheme is a realistic solution.

Author Contributions: Conceptualization, J.S. (Joe Sakai); funding acquisition and reviewing draft, J.S. (José Santiso); development of methodology, J.M.C.R.; performing films deposition, EDX and SEM analysis, and writing draft, J.S. (Joe Sakai); performing XRD analysis, J.P.-P.; performing XPS analysis, G.S.; performing AFM and PFM observation, P.V.-C. All authors have read and agreed to the published version of the manuscript.

Funding: This research was supported by Spanish Ministry of Competitiveness (projects MAT2016-77100-C2-1-P and PID2019-108573GB-C21) and the AGAUR agency (project 2017SGR). ICN2 is funded by the CERCA programme/Generalitat de Catalunya and by the Severo Ochoa programme of the Spanish Ministry of Economy, Industry and Competitiveness (MINECO, Grant No. SEV-2017-0706).

Institutional Review Board Statement: Not applicable.

Informed Consent Statement: Not applicable.

Data Availability Statement: The data presented in this study are available on request from the corresponding author.

Acknowledgments: The authors are grateful to Gustau Catalan, Ying Liu, Alba Fuentes, Francisco Javier Belarre Triviño, and Marcos Rosado Iglesias for their support on experiments.

Conflicts of Interest: The authors declare no conflict of interest.

References

1. Shirane, G.; Hoshino, S.; Suzuki, K. X-ray study of the phase transition in lead titanate. *Phys. Rev.* **1950**, *80*, 1105–1106. [CrossRef]
2. Jaffe, B.; Cook, W.R.; Jaffe, H. *Piezoelectric Ceramics*; Academic Press: London, UK, 1971.
3. Ueda, I.; Ikegami, S. Piezoelectric properties of modified $PbTiO_3$ ceramics. *Jpn. J. Appl. Phys.* **1968**, *7*, 236–242. [CrossRef]
4. Carl, K. Ferroelectric properties and fatiguing effects of modified $PbTiO_3$ ceramics. *Ferroelectrics* **1975**, *9*, 23–32. [CrossRef]
5. Norton, D.P. Pulsed laser deposition of complex materials: Progress toward applications. In *Pulsed Laser Deposition of Thin Films—Applications-led Growth of Functional Materials*; Eason, R., Ed.; A John Wiley & Sons, Inc.: Hoboken, NJ, USA, 2007; pp. 8–9.
6. Martín, M.J.; Mendiola, J.; Zaldo, C. Pulsed laser deposition of Sm modified $PbTiO_3$ ferroelectric thin films. *Ferroelectr. Lett.* **1997**, *22*, 101–105. [CrossRef]
7. Choi, T.; Lee, J. Structural and dielectric properties of artificial $PbZrO_3/PbTiO_3$ superlattices grown by pulsed laser deposition. *Thin Solid Films* **2005**, *475*, 283–286. [CrossRef]
8. Nishino, R.; Kozuka, Y.; Uchida, M.; Kagawa, F.; Kawasaki, M. Electrical conduction on the surface of ferroelectric $PbTiO_3$ thin film inducedby electrolyte gating. *Appl. Phys. Lett.* **2018**, *112*, 051602. [CrossRef]
9. Palkar, V.R.; Purandare, S.C.; Pai, S.P.; Chattopadhyay, S.; Apte, P.R.; Pinto, R.; Multani, M.S. *c*-axis oriented ferroelectric thin films of $PbTiO_3$ on Si by pulsed laser ablation. *Appl. Phys. Lett.* **1996**, *68*, 1582–1584. [CrossRef]
10. Wu, Y.M.; Lo, J.T. Growth of $PbTiO_3$ thin film on Si(100) with Y_2O_3 and CeO_2 buffer layer. *Jpn. J. Appl. Phys.* **1998**, *37*, 4943–4948. [CrossRef]
11. Seo, J.; Ahn, Y.; Kim, W.H.; Son, J.Y. Local ferroelectric responses of epitaxial $PbTiO_3$ thin films to heated atomic force microscopy. *Mater. Lett.* **2016**, *168*, 134–137. [CrossRef]
12. Li, S.; Zhu, Y.L.; Tang, Y.L.; Liu, Y.; Zhang, S.R.; Wang, Y.J.; Ma, X.L. Thickness-dependent a1/a2 domain evolution in ferroelectric $PbTiO_3$ films. *Acta Mater.* **2017**, *131*, 123–130. [CrossRef]
13. Lin, J.L.; Wang, Z.J.; Zhao, X.; Liu, W.; Zhang, Z.D. Microstructures and ferroelectric properties of $PbTiO_3/PbZrO_3$ superlattices deposited by pulse laser deposition. *Ceram. Int.* **2018**, *44*, 20664–20670. [CrossRef]

14. Shin, H.W.; Son, J.Y. Nonvolatile ferroelectric memory based on $PbTiO_3$ gated single-layer MoS_2 field-effect transistor. *Electron. Mater. Lett.* **2018**, *14*, 59–63. [CrossRef]
15. Feng, Y.; Tang, Y.; Ma, D.; Zhu, Y.; Zou, M.; Han, M.; Ma, J.; Ma, X. Thickness-dependent evolution of piezoresponses and stripe 90° domains in (101)-oriented ferroelectric $PbTiO_3$ thin Films. *ACS Appl. Mater. Interfaces* **2018**, *10*, 24627–24637. [CrossRef]
16. Christen, H.M.; Silliman, S.D.; Harshavardhan, K.S. Continuous compositional-spread technique based on pulsed-laser deposition and applied to the growth of epitaxial films. *Rev. Sci. Instrum.* **2001**, *72*, 2673–2678. [CrossRef]
17. Koinuma, H.; Takeuchi, I. Combinatorial solid-state chemistry of inorganic materials. *Nat. Mater.* **2004**, *3*, 429–438. [CrossRef]
18. Maruyama, S.; Kubokawa, O.; Nanbu, K.; Fujimoto, K.; Matsumoto, Y. Combinatorial synthesis of epitaxial $LiCoO_2$ thin films on $SrTiO_3$ (001) via on-substrate sintering of Li_2CO_3 and CoO by pulsed laser deposition. *ACS Comb. Sci.* **2016**, *18*, 343–348. [CrossRef]
19. Sakai, J.; Autret-Lambert, C.; Sauvage, T.; Courtois, B.; Wolfman, J.; Gervais, F. Epitaxial composition-graded perovskite films grown by a dual-beam pulsed laser deposition method. *J. Cryst. Growth* **2013**, *380*, 106–110. [CrossRef]
20. Sakai, J.; Roque, J.M.C.; Vales-Castro, P.; Padilla-Pantoja, J.; Sauthier, G.; Catalan, G.; Santiso, J. Control of lateral composition distribution in graded films of soluble solid systems $A_{1-x}B_x$ by partitioned dual-beam pulsed laser deposition. *Coatings* **2020**, *10*, 540. [CrossRef]
21. Hussey, B.W.; Gupta, A. Synthesis of $YBa_2Cu_3O_{7-d}$ films from separate oxide targets. *J. Appl. Phys.* **1992**, *72*, 287–289. [CrossRef]
22. Lee, Y.E.; Norton, D.P.; Budai, J.D. Enhanced photoluminescence in epitaxial $ZnGa_2O_4$: Mn thin-film phosphors using pulsed-laser deposition. *Appl. Phys. Lett.* **1999**, *74*, 3155–3157. [CrossRef]
23. Funakoshi, H.; Fumoto, K.; Okuyama, M.; Hamakawa, Y. Fabrication of lead titanate thin film by laser ablation with alternate deposition of lead oxide and titanium oxide precursors. *Jpn. J. Appl. Phys.* **1994**, *33*, 5262–5264. [CrossRef]
24. Koster, G.; Kropman, B.L.; Rijnders, G.J.H.M.; Blank, D.H.A.; Rogalla, H. Quasi-ideal strontium titanate crystal surfaces through formation of strontium hydroxide. *Appl. Phys. Lett.* **1998**, *73*, 2920–2922. [CrossRef]
25. Doughty, C.; Findikoglu, A.T.; Venkatesan, T. Steady state pulsed laser deposition target scanning for improved plume stability and reduced particle density. *Appl. Phys. Lett.* **1995**, *66*, 1276–1278. [CrossRef]
26. Dam, B.; Rector, J.; Chang, M.F.; Kars, S.; de Groot, D.G.; Griessen, R. Laser ablation threshold of $YBa_2Cu_3O_{6+x}$. *Appl. Phys. Lett.* **1994**, *65*, 1581–1583. [CrossRef]
27. Hase, T.; Hirata, K.; Amanuma, K.; Hosokawa, N.; Miyasaka, Y. Preparation of Pb(Zr, Ti)O_3 thin films by multitarget sputtering. *Jpn. J. Appl. Phys.* **1994**, *33*, 5244–5248. [CrossRef]